

# A New Transmission Line Protection Approach Using Cumulants and Artificial Neural Networks

Janison R. de Carvalho · Denis V. Coury ·  
Carlos A. Duque · Bruno F. Paula

Received: 13 March 2012 / Revised: 21 August 2012 / Accepted: 25 February 2013 / Published online: 6 January 2014  
© Brazilian Society for Automatics–SBA 2014

**Abstract** This article presents a new methodology for transmission line protection that uses higher-order statistics (HOS), cumulants, and artificial neural networks (ANNs). The main objective is to design a distance relay algorithm. Results for the fault-detection and -classification stages are presented, as well as for fault location. The proposed method combines a large number of samples of cumulants with different features and the capability of ANNs to discriminate different patterns. In summary, HOS are used for feature extraction in the protection scheme. The ANNs receive these statistics as inputs, and they are responsible for the logical functioning of the protection system, deciding if a trip is needed after detecting, classifying, and locating a fault. The results have shown that the proposed approach is suitable for protection purposes. For the fault-detection stage, results have shown to be immune to the high presence of additive noise and also to the power-system frequency deviation. Moreover, the fault-classification stage is computed without the need of current information from the power system. Finally, the preliminary results for fault location are precise for a correct estimation of fault distance and determination of the fault zone. It must be highlighted that this new distance protection approach is

essentially based on voltage signals, using current signals only for determining the direction of the fault. This fact represents an innovation in distance relaying.

**Keywords** Transmission line protection · Higher-order statistics · Artificial neural networks

## 1 Introduction

Transmission lines (TLs) are components of fundamental importance in an electric power system (EPS), and they are the only way of carrying electric energy. They are the largest part of the transmission system and hence the majority of faults are located on them. In this context, protection schemes play an important role in eliminating a fault as quickly as possible and in providing the isolation of the minimum portion of the electric network (Caminha 1977).

A complete model of distance protection of transmission lines is shown in Fig. 1. This protection is described in the following three steps:

- *Fault Detection*: This stage consists of identifying the occurrence of the fault;
- *Fault Classification*: This stage indicates the type of fault, i.e., it identifies the phases involved in the disturbance, as well as the presence of ground;
- *Fault Location*: This stage is responsible for estimating the distance  $d$  between the fault and the relay locations.

Several algorithms for the digital protection of TLs being currently used are based on the estimation of the apparent impedance (Coury et al. 2007). The performance of such methods is directly related to the accuracy and precision of

---

J. R. de Carvalho · B. F. Paula  
Federal Center of Technological Education of Minas Gerais  
(CEFET-MG/Campus III), R. José Peres 558, Centro, Leopoldina,  
MG CEP 36.700-000, Brazil

J. R. de Carvalho · D. V. Coury (✉)  
Electrical and Computer Engineering Department, São Carlos  
School of Engineering, University of São Paulo (USP),  
Av. Trabalhador São-Carlense, 400 Centro, São Carlos,  
SP CEP 13.566-590, Brazil  
e-mail: coury@sc.usp.br

C. A. Duque  
Electrical Engineering Department, Federal University of Juiz  
de Fora (UFJF), Juiz de Fora, MG CEP 36036-330, Brazil

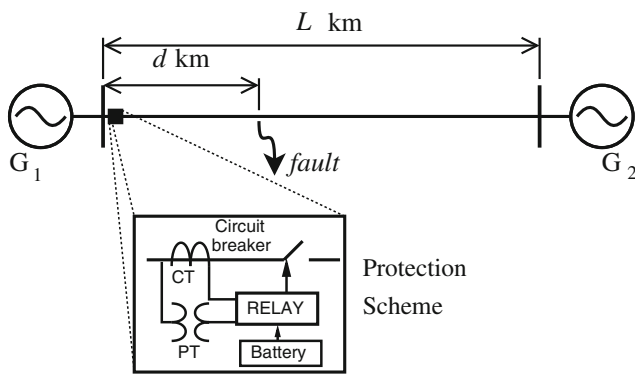


**Fig. 1** An electric power system with a fault in a transmission line,  $d$  km far from the relay

those techniques used in phasor estimations of fundamental components of current and voltage signals. Thus, some of the methods proposed in the literature deal with negative aspects of phasor estimations such as errors due to fundamental frequency drifting, the presence of noise in the signals, the presence of DC exponential decaying component, the length of the data window used in analysis, etc. (Phadke et al. 1983; Sá and Pedro 1991; Eichhorn et al. 1993; Alfuhaid and El-Sayed 1999; Grcar et al. 2008; Chen et al. 2006; Yu 2006; Cho et al. 2009).

New methods have been proposed in the literature for protection purposes in EPS based on alternative approaches such as artificial intelligence techniques. The use of genetic algorithms, intelligent agents, and artificial neural networks (ANNs) should be emphasized (Coury et al. 2011). Talking specifically about neural networks, the use of this tool in solving problems in EPS has been published since 1990 (Khaparde et al. 1991; Jongepier and Sluis 1997; Dalstein and Kuliche 1995; Coury and Jorge 1998; Osman et al. 2005; Zhang and Kezunovic 2007; Dutta and Kadu 2010). ANNs are computational models inspired by the human brain, and the interest in this technique is related to its useful properties and characteristics, such as (Silva et al. 2010) the following:

- Learning by means of examples;
- Adaptive capability;
- Generalization capability;
- Fault tolerance; and
- Clustering capability.

The use of higher-order statistics (HOS) in power quality (PQ) issues concerning detection and classification of disturbances motivated this study. Ribeiro et al. (2007) deals specifically with the problem of detection of PQ disturbances aiming at an automatic monitoring system capable of storing data windows containing electric signals. Gerek and Ece (2006) and Ferreira et al. (2009) deal with the problem of disturbance classification. The aim of these articles is an

automatic system which can identify the type of disturbance which occurred in the electric signals. In the protection field, the use of HOS in classification of faults of TLs with series compensation should be mentioned (Pradhan et al. 2004)

In this study, the present authors use HOS of electric signals for feature extraction. The statistics used are cumulants, and they are obtained from sliding data windows. The cumulants are the inputs of ANNs used in the scheme. Inherent characteristics of HOS, such as noise immunity, the large number of statistics, among others, classify the method as appropriate for transmission line protection purposes. The article is organized as follows. Section 2 presents a brief introduction to HOS and ANNs. Section 3 describes the proposed protection system. The simulated power system and the results are shown and discussed in Sect. 4. Finally, Sect. 5 presents the concluding remarks.

## 2 Higher-Order Statistics and Artificial Neural Networks

This section provides a succinct and objective description of the two tools used in this study.

### 2.1 Higher Order Statistics

The use of HOS has been reported to solve detection problems, as in Giannakis and Tsatsanis (1990) and Colonnese and Scarano (1999). More precisely in the early 1990s, there was a wide interest in these statistics and their applications (Mendel 1991). They provide more information about a process, compared with the information of mean values and variance (Marques 2007). Thus, it can be expected that they have a better way of discriminating patterns in some applications. The HOS are defined in terms of *moments* and *cumulants* of higher order. The latter ones are the statistics used in this study. In this section, the definitions of cumulants are presented based on the theory available in Mendel (1991) and on the considerations by Marques (2007).

Let  $X$  be a stochastic process with  $n$  random variables  $(x_1, x_2, \dots, x_n)$ . Real-valued random variables with zero mean have cumulants of the 2nd-, 3rd-, and 4th-order defined as (Mendel 1991),

$$\begin{aligned} \text{cum}(x_1, x_2) &= E(x_1 x_2), \\ \text{cum}(x_1, x_2, x_3) &= E(x_1 x_2 x_3), \\ \text{cum}(x_1, x_2, x_3, x_4) &= E(x_1 x_2 x_3 x_4) - E(x_1 x_2)E(x_3 x_4) \\ &\quad - E(x_1 x_3)E(x_2 x_4) \\ &\quad - E(x_1 x_4)E(x_2 x_3), \end{aligned} \quad (1)$$

where  $E(\cdot)$  is the expectation operator. Supposing  $\{x(t)\}$  a stationary random process with zero mean, its  $k$ th-order cumulants can be defined in terms of signals  $x(t)$ ,  $x(t +$

$\tau_1), \dots, x(t + \tau_k)$ , Thus, from (1), the cumulants can be rewritten as

$$\begin{aligned} C_{2,x}(\tau_1) &= E \{x(t)x(t + \tau_1)\}, \\ C_{3,x}(\tau_1, \tau_2) &= E \{x(t)x(t + \tau_1)x(t + \tau_2)\}, \\ C_{4,x}(\tau_1, \tau_2, \tau_3) &= E \{x(t)x(t + \tau_1)x(t + \tau_2)x(t + \tau_3)\} \\ &\quad - C_{2,x}(\tau_1)C_{2,x}(\tau_2 - \tau_3) \\ &\quad - C_{2,x}(\tau_2)C_{2,x}(\tau_3 - \tau_1) \\ &\quad - C_{2,x}(\tau_3)C_{2,x}(\tau_1 - \tau_2), \end{aligned} \tag{2}$$

where  $\tau_1, \dots, \tau_3$  are time lags (or, simply, *lags*) and  $C_2, C_3,$  and  $C_4$  are, respectively, the cumulants of 2nd-, 3rd-, and 4th-order. Assuming a single time lag  $\tau_1 = \tau_2 = \tau_3 = \tau$ , the following can be obtained:

$$\begin{aligned} C_{2,x}(\tau) &= E \{x(t)x(t + \tau)\}, \\ C_{3,x}(\tau) &= E \left\{ x(t)x^2(t + \tau) \right\}, \\ C_{4,x}(\tau) &= E \left\{ x(t)x^3(t + \tau) \right\} - 3C_{2,x}(\tau)C_{2,x}(0). \end{aligned} \tag{3}$$

If the analyzed signal is a  $N$ -length discrete sequence  $\{x[n]\}$ , then (3) can be approximated (Marques 2007) as follows:

$$\begin{aligned} C_{2,x}(\tau) &= \frac{1}{N/2} \sum_{k=0}^{N/2-1} x[k]x[k + \tau], \\ C_{3,x}(\tau) &= \frac{1}{N/2} \sum_{k=0}^{N/2-1} x[k]x^2[k + \tau], \\ C_{4,x}(\tau) &= \frac{1}{N/2} \sum_{k=0}^{N/2-1} x[k]x^3[k + \tau] \\ &\quad - \frac{3}{(N/2)^2} \sum_{k=0}^{N/2-1} x[k]x[k + \tau] \cdot \sum_{n=0}^{N/2-1} x^2[n]. \end{aligned} \tag{4}$$

The use of (4) is responsible for a loss of information because a few samples of signal  $x[n]$  are not used in computation of cumulants. In fact, if  $k$  exceeds  $N/2 - 1$ , then  $k + \tau$  exceeds the length of the input signal. Thus, the strategy used in Marques (2007) is to provide a circular shift in such a way that all samples are used in computation of (4). Mathematically, this operation can be represented by

$$\text{mod}(k + \tau, N) = (k + \tau) - bN, \tag{5}$$

where  $b$  is the integer number obtained from the division of  $k + \tau$  by  $N$ . Thus, the following can be obtained:

$$\begin{aligned} C_{2,x}(\tau) &= \frac{1}{N} \sum_{k=0}^{N-1} x[k]x[\text{mod}(k + \tau, N)], \\ C_{3,x}(\tau) &= \frac{1}{N} \sum_{k=0}^{N-1} x[k]x^2[\text{mod}(k + \tau, N)], \\ C_{4,x}(\tau) &= \frac{1}{N} \sum_{k=0}^{N-1} x[k]x^3[\text{mod}(k + \tau, N)] \\ &\quad - \frac{1}{N^2} \sum_{k=0}^{N-1} x[k]x[\text{mod}(k + \tau, N)] \cdot \sum_{k=0}^{N-1} x^2[k]. \end{aligned} \tag{6}$$

In Eq. (6),  $\tau = 0, 1, \dots, N - 1$ . These equations, in association with ANNs, are the basis of the proposed method to detect and classify faults in transmission lines. Finally, it is important to mention that cumulants provide higher-order correlations of a process, and they are also a measure of the “distance” of the process from a Gaussian process with the same mean and variance (Mendel 1991). In fact, the cumulants with an order higher than two are all zero for Gaussian processes.

In order to exemplify the application of HOS in detection problems, let us consider the signals of Fig. 2. In (a), a sinusoidal electric signal is presented, and in (b), the signal consists of a high-frequency oscillatory decaying component superimposed on a sinusoidal signal component. Thus, the latter signal presents a PQ transient event normally due to switching of capacitor banks. Let us consider the application of eq. (6) in the two data windows specified in the figure. Marques (2007) demonstrated that the cumulants can provide features for discriminating signals with and without disturbances as shown in Fig. 3. More specifically, the 2nd-order cumulant with lags 17 and 32 and the 4th-order cumulant with lag 2 were used. It should be mentioned that the representation of cumulants of Fig. 3 was obtained considering several PQ disturbances instead of the transients represented in Fig. 2 uniquely.<sup>1</sup>

### 2.2 Artificial Neural Networks

Artificial neural networks (ANNs) can be defined as a set of processing units (neurons) interconnected by a large number of connection links (synapses) (Silva et al. 2010). Mathematically, the synapses are weights and are responsible for storing information, in other words, for the learning process of the network.

Among all applications of ANN, a majority of them are concentrated on pattern’s recognition and function approximation. In the former, the network must evaluate the pattern at the inputs recognizing its respective class from the predefined

<sup>1</sup> Figure from Marques (2007).

**Fig. 2** Electric signals **a** pure sinusoidal; **b** pure sinusoidal with high-frequency transient

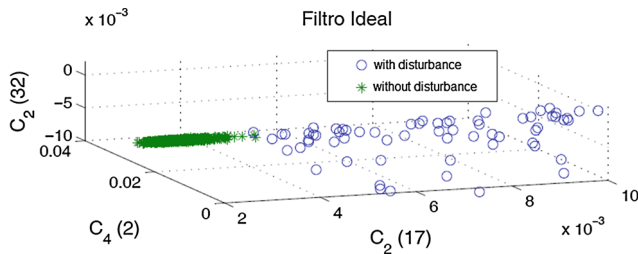
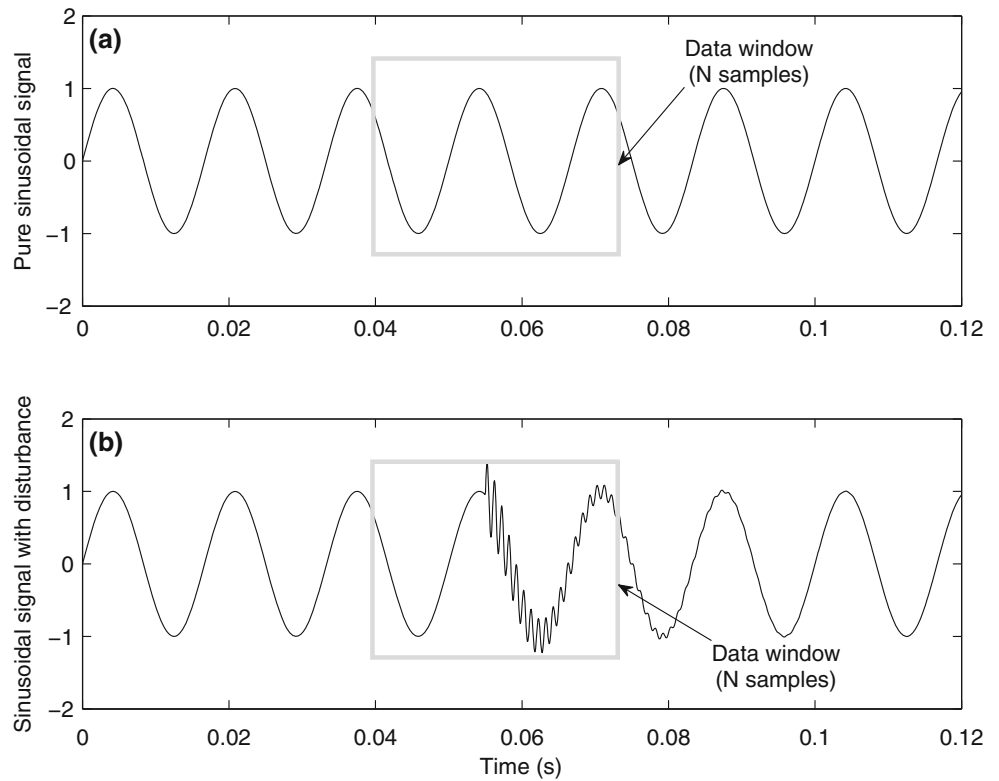


**Fig. 3** Using cumulants for discriminating signals with power-quality disturbances

ones. In function approximation, the network must estimate an output for the data at the inputs, performing the function of an arbitrary system.

A model for the basic processing unit of an ANN (the neuron) is represented in Fig. 4. The inputs  $x_1, \dots, x_N$  are multiplied by their respective synaptic weights  $w_1, \dots, w_N$ , and the results are added, including the term  $\theta$ , in the linear combiner. This parameter is the threshold for the activation of the neuron. The output of the linear combiner,  $u$ , is the input of the activation function,  $g(\cdot)$ , resulting in the neuron output,  $y$ . Mathematically,

$$\begin{cases} u = \sum_{i=1}^N w_i x_i - \theta, \\ y = g(u). \end{cases} \quad (7)$$

Considering the input  $x_0 = -1$ , the threshold  $\theta$  can be represented by a weight  $w_0$ , i.e.,

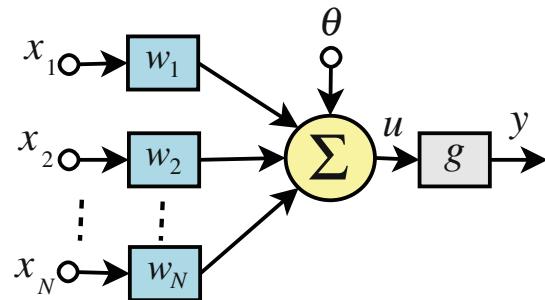


**Fig. 4** Neuron model (Perceptron)

$$\begin{cases} u = \sum_{i=0}^N w_i x_i, \\ y = g(u). \end{cases} \quad (8)$$

In engineering problems, most applications of neural networks use Multilayer Perceptron (MLP). They are *Feedforward* networks with an input layer ( $x_1, \dots, x_N$ ), at least one hidden layer, and an output layer. All these layers are specified in Fig. 5 considering an MLP with two neuron layers:  $N$  input signals compose the input,  $N_1$  neurons are present in the hidden layer, and  $N_2$  neurons are present in the output layer. Each circle represents the sum block and activation function of a basic neuron of Fig. 4.

The MLP belongs to the ANN class concerning supervised learning. This means that this network can be applied to problems in which a set of inputs,  $x_1(k), \dots, x_N(k)$ , and

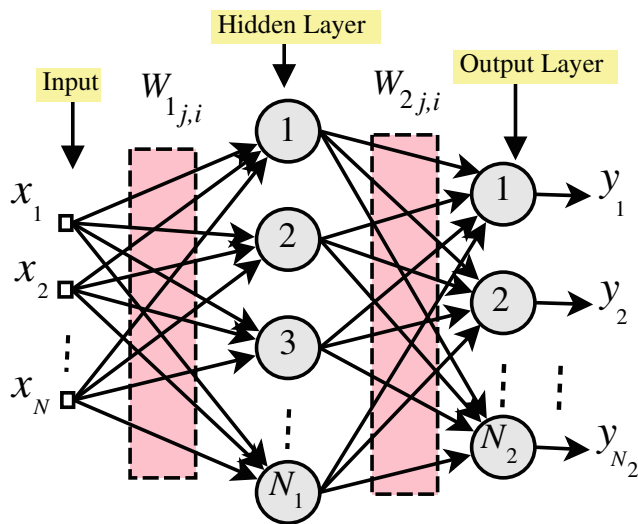


Fig. 5 Perceptron with two layers

its respective set of outputs,  $d_1(k), \dots, d_{N_2}(k)$ , are available. The learning process is carried out adjusting the weight matrixes so that the  $k$ th pattern at the input produces an output  $y_j(k)$  approximately equal to the desired output  $d_j(k)$  ( $j = 1, \dots, N_2$ ).

The training process of MLP is performed using the *Backpropagation* algorithm (Haykin 1999), also known as the Generalized Delta Rule. In the middle of the 1980s, this algorithm was responsible for restarting research in ANNs (Silva et al. 2010). The algorithm consists of two steps:

- *Forward* The data are applied at the input of the ANN, and the signals are diffused through it interacting with the synaptic weights;
- *Backward* From the resulting outputs  $y_j(k)$ , an error is calculated and diffused back to adapt the weight matrixes.

The process of adapting weights is performed by means of the Gradient of the squared error:

$$E(k) = \frac{1}{2} \sum_{j=1}^{N_2} [d_j(k) - y_j(k)]^2. \tag{9}$$

Because of the use of the gradient, the transfer functions must be differentiable. The use of the log-sigmoid transfer function can be highlighted, given by

$$g(u) = \frac{1}{1 + e^{-\beta_{RNA} u}}, \tag{10}$$

where the  $\beta_{RNA}$  factor describes the range of transition of the function. This function takes the input, which can have any value between plus and minus infinity, and limits the output in the range from 0 to 1.

A general equation for adapting the weight connecting the  $j$ th neuron of the current layer to the its  $i$ th input can be written as

$$w_{ji}(t + 1) = w_{ji}(t) + \eta \delta_j y_i, \tag{11}$$

where  $\eta$  is the learning rate,  $\delta_j$  is the local gradient of neuron  $j$ , and  $w_{ji}(t)$  and  $w_{ji}(t + 1)$  are the weights at epochs  $t$  and  $t + 1$ , respectively. In this study, the Levenberg–Marquardt algorithm was adopted for the training process. This algorithm combines gradient descent with the Newton’s method. This is chosen because this method makes use of second-order gradients and is consequently responsible for a faster training process (10–100 times faster than the traditional *Backpropagation* algorithm). The improved characteristics of convergence of the algorithm are related to the use of the Hessian Matrix. More details of the *Backpropagation* and Levenberg–Marquardt algorithms can be found in Silva et al. (2010) and Haykin (1999).

### 3 The Proposed Protection Scheme

#### 3.1 General Description of the Protection Scheme

The general structure for TL protection using cumulants and neural networks is shown in Fig. 6. The connection of the three main blocks should be mentioned: Fault-Detection, -Classification, and -Location Stages. Initially, the operation of the fault-detection stage only should be emphasized. This block has the voltage signals as its inputs. If the system operates normally, i.e., without the occurrence of a fault, then this is the only subsystem in operation. It provides the EPS monitoring and must indicate a faulty condition immediately after its inception. It can be observed that the method uses voltage signals only in this process. A dedicated ANN is used in this step to recognize the pre and postfault conditions. With the inception of a fault, the detection subsystem enables a counter and waits until a predefined threshold is attained, confirming the faulty condition. At this time, the detection subsystem is disabled, and the fault-classification one is started.

The fault-classification subsystem has ten outputs, each one equivalent to one of the faults considered in this study: (a) Phase-to-Phase faults (Ph–Ph), including A–B, B–C, and C–A faults; (b) Phase-to-Ground faults (Ph–G), including A–G, B–G, and C–G faults; (c) Phase-to-Phase-to-Ground faults (Ph–Ph–G), including A–B–G, B–C–G, and C–A–G faults; and, finally Phase-to-Phase-to-Phase fault (Ph–Ph–Ph), i.e., A–B–C. This stage also uses a counter to register the number of consecutive samples to indicate the type of fault.

After disabling the fault-classification stage, the fault-location stage is enabled. This latter subsystem is divided into four parts, with each one being responsible for each type of fault, as specified before:

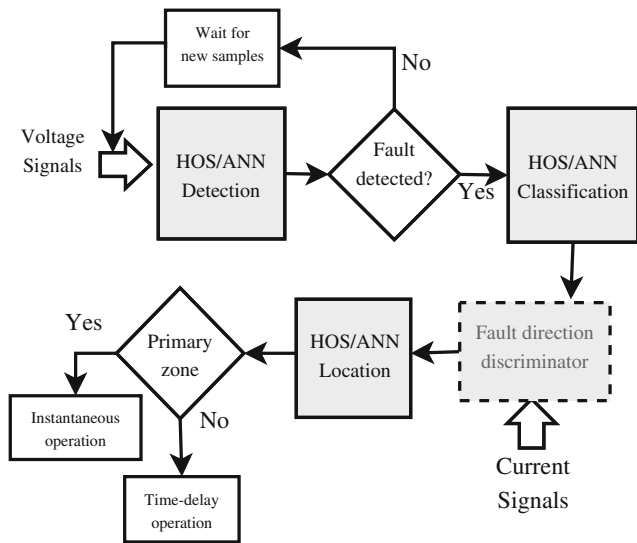


Fig. 6 Protection scheme proposed in this study

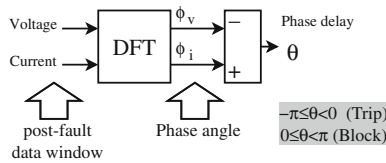


Fig. 7 Fault direction algorithm

Ph–Ph, Ph–G, Ph–Ph–G, and Ph–Ph–Ph: The output of this block consists of an estimation of the fault distance measured from the relay location.

Depending on the power-system configuration, a directional algorithm should precede the location stage, as shown in Fig. 6. In this study, a simple and traditional method to distinguish the direction of fault was used (Phadke and Thorp 2009). The method is based on the analysis of phase angles of electric signals extracted from the faulty phase. Using the traditional Discrete Fourier Transform (DFT) for phasor estimations, the representation of the directional algorithm is shown in Fig. 7. As demonstrated in Phadke and Thorp (2009), there are two possible conditions (trip or block) for the phase angle  $\theta$  (between current and voltage signals in a faulty phase), as shown in the figure.

### 3.2 Description of the System Components

The three subsystems of the proposed method (fault detection, classification, and location) can be represented by only one block diagram. This diagram is shown in Fig. 8. As can be observed, there are three stages to be executed: (a) the filtering stage; (b) the HOS computation stage; and (c) the ANN stage. More specifically, the filtering stage is common to all the subsystems. In contrast, the HOS and ANN stages

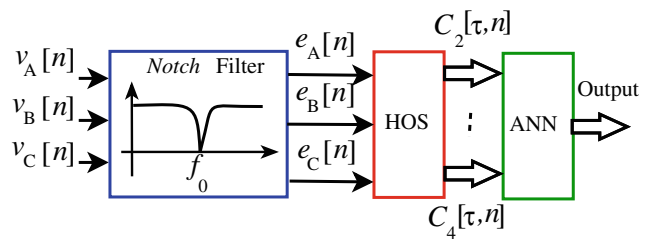


Fig. 8 General structure for fault-detection, -classification, and -location stages

are particular and specific for each subsystem of the proposed method.

The process of detecting, classifying, and locating a fault starts with the application of parameterized notch filters to voltage signals. The transfer function of these filters is given by (Mitra 2006)

$$H(z) = \frac{1 + \alpha}{2} \cdot \frac{1 - 2\beta z^{-1} + z^{-2}}{1 - \beta(1 + \alpha)z^{-1} + \alpha z^{-2}}. \tag{12}$$

This filter is designed to completely remove the fundamental component of the electric signal ( $f_0 = 60$  Hz). Parameter  $\beta$  controls the position of the notch frequency, and parameter  $\alpha$  controls the length of the rejection band. The outputs of these filters are defined as error signals, and the use of such signals is based on the fact that several detection techniques are based on error signals. In normal operations, the signals in the EPS are sinusoidal and, consequently, the outputs of equation (12) are zero or possibly a noisy component.

Thus, the following formulation can be introduced to represent the problem under study. This formulation is based on two hypotheses,

$$\begin{aligned} H_0 : e_v[n] &= r_v[n], \\ H_1 : e_v[n] &= r_v[n] + t_v[n], \end{aligned} \tag{13}$$

where  $v = \{A, B, C\}$  represents each one of the three phases of the EPS. The noise signal  $r_v[n]$  is a Gaussian component and  $t_v[n]$  is a transient component. The null hypothesis  $H_0$  is associated with normal operation conditions of the protected transmission line. On the other hand, the alternative hypothesis  $H_1$  is associated with the faulty condition.

After the filtering stage, the HOS are computed for  $N$ -length sliding windows of error signals ( $e_A, e_B$  e  $e_C$ ). In this study, it was decided to investigate only the 2nd- and 4th-order cumulants. Marques (2007) found out that the 3rd-order cumulants were not significant for problems involving Power Quality. In addition, as stated by Mendel (1991), some distributions have lower 3rd-order cumulants. Thus, at time instant  $n$ , the outputs of the second stage are

$$\begin{aligned}
 C_{2,v}(\tau, n) &= \begin{bmatrix} C_{2,v}(0, n) \\ C_{2,v}(1, n) \\ \vdots \\ C_{2,v}(N-1, n) \end{bmatrix}; \\
 eC_{4,v}(\tau, n) &= \begin{bmatrix} C_{4,v}(0, n) \\ C_{4,v}(1, n) \\ \vdots \\ C_{4,v}(N-1, n) \end{bmatrix}.
 \end{aligned} \tag{14}$$

In (14), index  $v$  can assume any value of the set  $\{A, B, C\}$ , representing a specific phase in analysis. Therefore, it can be concluded that certain amounts of  $N$  2nd-order cumulants and  $N$  4th order cumulants are available, per phase, to be used in fault- detection, -classification, and -location subsystem. Hence, it must be emphasized that there is a large number of statistics available for implementing the operation logic of the proposed relay. However, only a small portion of these statistics are actually used. The choice of the subset of cumulants used in the proposed algorithm obeys some criterion of the parameter selection that is not considered in the present study.

Some combinations of cumulants of phases  $A, B,$  and  $C$  consist of the input of the third and last stage. This stage is composed of neural networks. Each subsystem has a specific ANN using an MLP architecture. For fault-detection and -classification stages, the network performs pattern recognition functions. In the first case, the ANN must identify the faulty and nonfaulty conditions and only one output is sufficient to this process. In the second case, the ANN must identify the type of fault, and ten outputs are necessary for this task. Finally, the location stage applies neural networks performing function approximations. In other words, for a certain combination of cumulants as its inputs, the network must provide an estimation of the fault distance from the relay location. For this task, only one output is needed.

### 3.3 Obtaining Data for ANN Training

The general principle adopted for the development of the three subsystems (fault detection, classification, and location) is presented in Fig. 9. It can be observed from the discussion above, that the three stages operate consecutively. Thus, the samples are divided into three groups or datasets as shown in Fig. 9. The first partition is used for implementing the fault detection stage, aiming at speed and reliability. The second dataset is used in the development of the fault-classification stage. Finally, the last partition is used in development of the fault-location stage. Since the fault-classification stage is performed before the fault-location stage, four different sys-

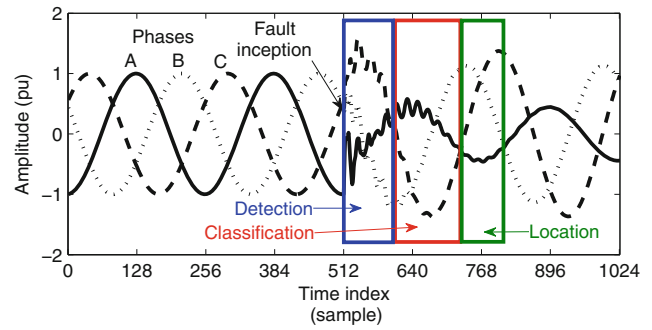


**Fig. 9** Window division of postfault electric signals for detecting, classifying, and locating faults using the proposed structure

tems for locating faults can be used, each one specialized in one type of fault considered in this study.

The strategy of partitioning the data aims at simplifying the protection stages without degrading their performance. The lengths of windows of Fig. 9 do not obey a specific rule but should be as short as possible. For instance, lengths which are fractions of one period of fundamental component could be used. The design of the fault-detection module also uses a dataset before the fault inception for correctly identifying the pre and postfault conditions.

## 4 Simulation Results

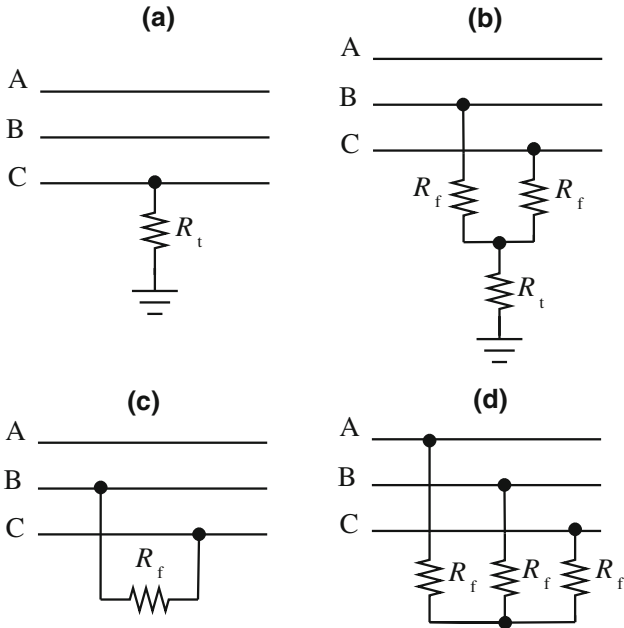
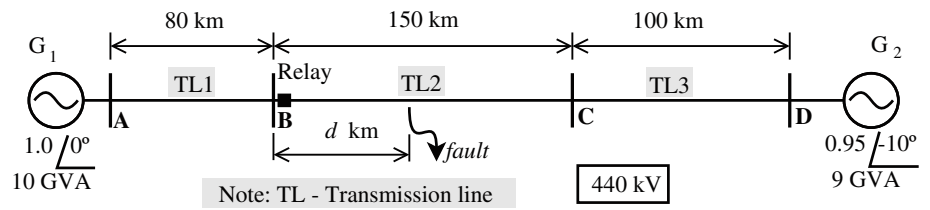
### 4.1 The EPS Studied

Figure 10 shows the simulated EPS which consists of three transmission lines. Line 1 is 80 km long and is located between busbars A and B. Line 2 is 150 km long and is located between busbars B and C. This line is the focus of the present article, and the relay is located at busbar B for protection of this part of the EPS. Finally, Line 3 is located between busbars C and D and is 100 km long.

Simulink/Matlab<sup>®</sup> was used in the simulations. The faults were implemented with a phase-to-phase (Ph–Ph) fault resistance  $R_f$  and a phase-to-ground (Ph–G) fault resistance  $R_t$ , as shown in Fig. 11. Typical signals of fault simulations using this software are presented in Fig. 12. In this case, signals of a fault involving phase A and Ground (A–G fault) are presented, 45 km far from the busbar B. In all simulations, ideal models for current and potential transformers are used.

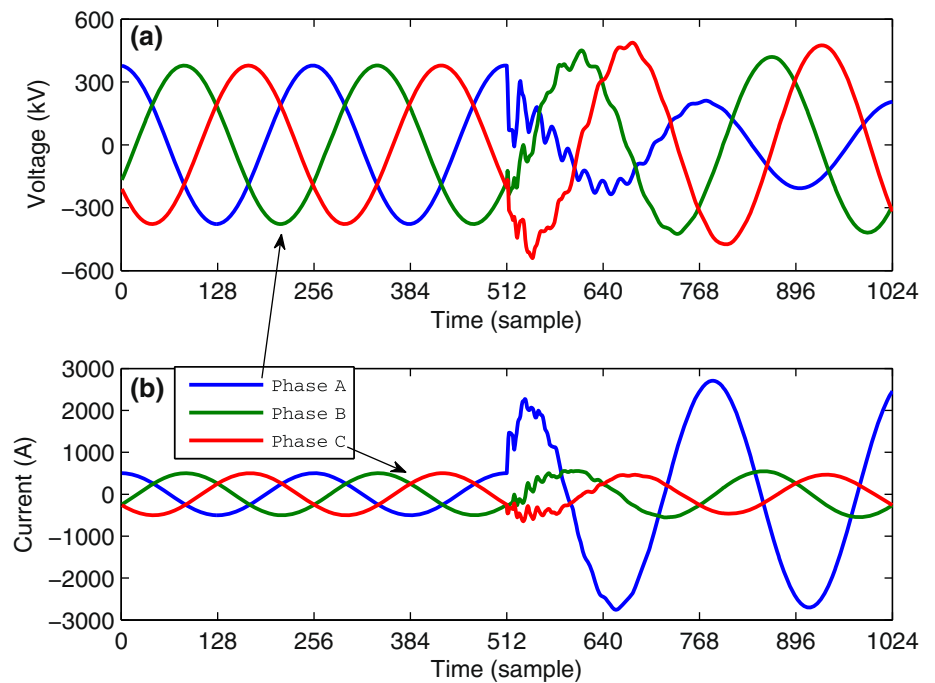
The fault conditions were obtained by varying the following parameters: (a) distance  $d$  between the relay position and the fault location; (b) the fault resistances; (c) the fault inception angle; and (d) the type of fault. Table 1 shows the values considered for each one of the aforementioned parameters. It can be noticed that a total of 6,264 distinct cases of faults are available for this study. Finally, the sampling rate used in all simulations is  $f_s = 256 \times f_0$  Hz.

**Fig. 10** The electric power system simulated



**Fig. 11** Electric connections for simulating faults

**Fig. 12** Electric signals of **a** voltages and **b** currents for a fault at Line 2, 45 km far from the busbar B and involving the phase A and Ground (A–G)



### 4.2 Fault-Detection Stage

A large dataset was generated initially considering the EPS operating with nominal frequency  $f_0 = 60$  Hz. From the total number of cases, the following values were used to generate data for the neural network training:  $d = \{5, 25, \dots, 145\}$  km,  $\phi = \{0^\circ, 90^\circ, 120^\circ, 210^\circ\}$ ,  $R_t = \{0.1, 100\}$   $\Omega$  and  $R_f = \{0.01, 10\}$   $\Omega$ . The results of the fault-detection stage were compared to the results of traditional sample-to-sample and cycle-to-cycle comparison techniques (Mohanty et al. 2008).

The cumulants were computed considering sliding data windows with a quarter of the fundamental cycle, i.e., 64 samples. The 32 samples before the fault inception formed the pre-fault class. The post-fault class was also formed by 32 samples collected from the 64th sample after the fault inception. Thus, the patterns were generated without mixing voltage samples of pre and post-fault conditions. This strategy facilitates the task of class discrimination and provides reliability to the process.

A combination of the 4th-order cumulants used in the fault-detection stage is shown in Fig. 13. In this figure,

**Table 1** Parameters for simulating faults

Fault type	Location (km)	Inception angle (°)	Fault resistance (Ω)
F–G	5, 10, . . . , 145	0, 30, . . . , 330	$R_T = 0.1, 1.0, 10, 100, 400$
F–F	5, 10, . . . , 145	0, 30, . . . , 330	$R_F = 0.1, 1, 10, 50$
F–F–G	5, 10, . . . , 145	0, 30, . . . , 330	$R_T = 0.1, 1.0, 10, 100, 400$
F–F–F	5, 10, . . . , 145	0, 30, . . . , 330	$R_F = 0.1, 1, 10, 50$

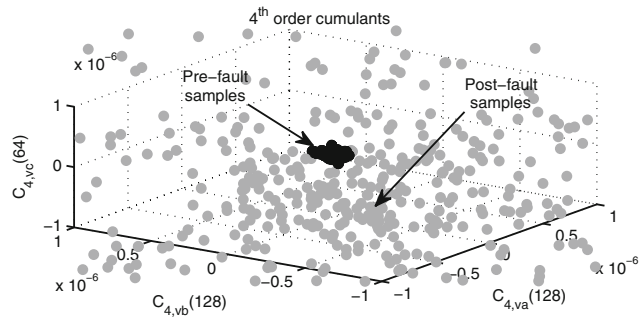


**Fig. 13** Representation of patterns of pre and postfault conditions in a cumulant space for the three phases

cumulants of prefault condition (black patterns) and postfault condition (gray patterns) can be seen. The data in this figure were generated considering the addition of white Gaussian noise-to-voltage signals with SNR (Signal-to-Noise Ratio) of 35 dB.

A neural network consisting of three inputs and two neural layers was trained to recognize classes in Fig. 13. The first neural layer has  $N_1 = 6$  neurons, and the output neural layer has  $N_2 = 1$  neuron. A quantum of 90 % of data was used in the training process, and the mean squared error (MSE) was 0.00259 after 3,000 epochs of training. The remaining 10 % of data was used in the validation process. The hit rate in this process was 98 %.

A particular result of fault detection, considering a C–A–G fault with  $d = 70$  km,  $R_f = 0.01 \Omega$ ,  $R_t = 0.1 \Omega$ , and  $\phi = 90^\circ$ , is shown in Fig. 14. In (a) the electric signals are presented. The cumulants are shown in (b). The fault is simulated at sample 128, and the fault detection of the event by the proposed method is shown in (c). In (d), the results of cycle-to-cycle ( $s_c$ ) and sample-to-sample ( $s_a$ ) comparison techniques are presented, considering the voltage of phase A. Fault detection using the  $s_a$  and  $s_c$  indexes of these two techniques needs a threshold for comparison. In the proposed technique, the neural network performs all the tasks concerning analyzing the signals, and no threshold is needed.

A second fault situation is carried out considering the EPS operating with frequencies different from the nominal frequency  $f_0 = 60$  Hz. The frequency values in these simulations are {59; 59, 5; 60, 5; 61} Hz. Moreover, the voltage signals are considered to be a sinusoidal signal superimposed

with white Gaussian noise component (SNR) = 35 dB. The same topology of neural network is used to obtain a new fault-detection stage. In Fig. 15, a particular result for a fault involving phases C and A (A–C fault) is shown considering  $d = 35$  km,  $R_f = 0.1 \Omega$ ,  $\phi = 120^\circ$ ,  $f = 61$  Hz and SNR = 30 dB. It can be observed that this situation degrades the performance of traditional techniques if compared with the result of the proposed algorithm. As can be seen, the proposed method is capable of detecting the fault in the presence of noise and frequency drifting.

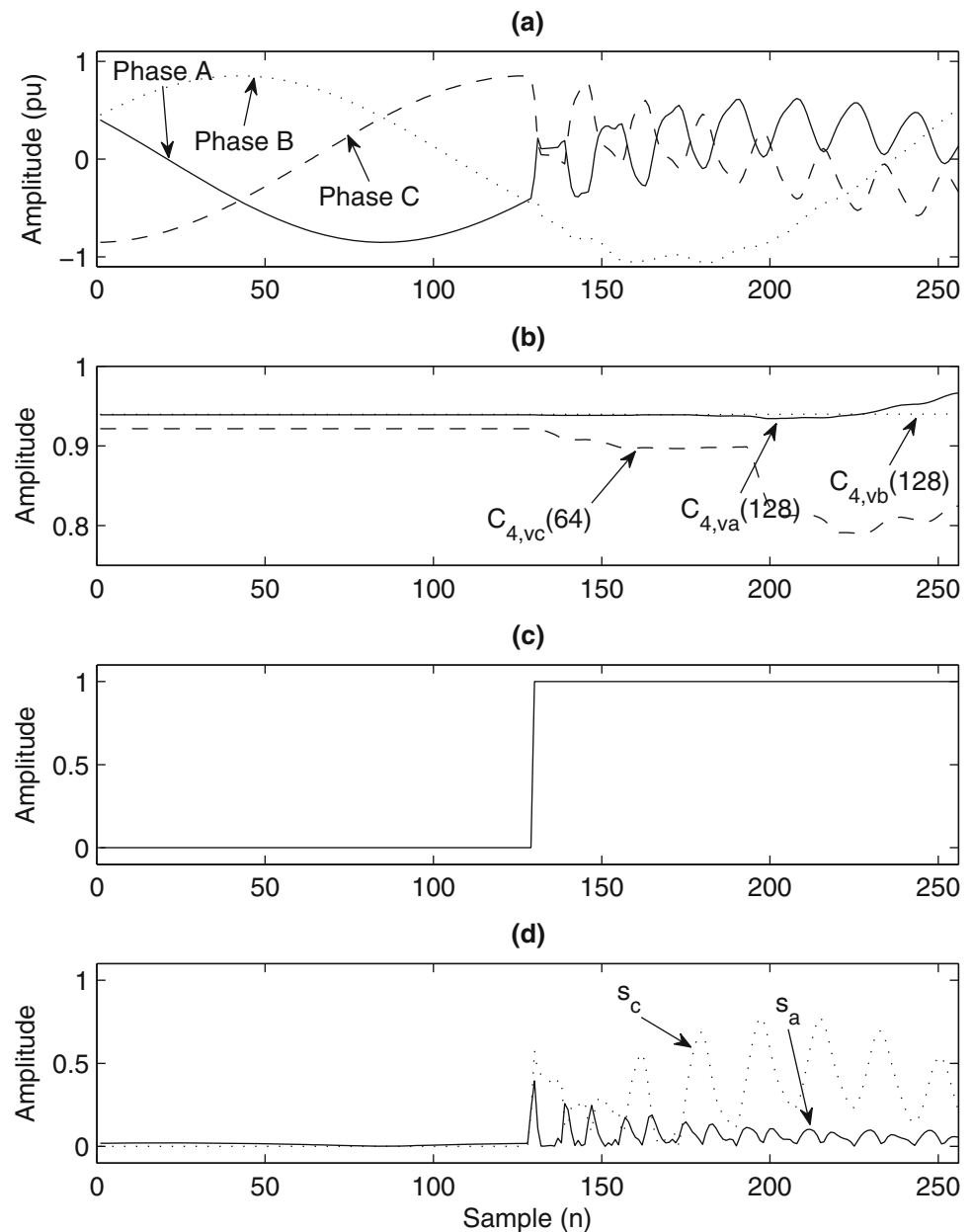
### 4.3 Fault-Classification Stage

After the fault-detection stage, the next step is to classify the fault. Considering the EPS operating with nominal frequency ( $f = 60$  Hz), the following parameters were used for generating training data:  $d = \{5, 30, \dots, 140$  km},  $\phi = \{0^\circ, 30^\circ, \dots, 330^\circ\}$ ,  $R_t = \{0.1, 1, 100, 400 \Omega\}$  e  $R_f = \{0.1, 10 \Omega\}$ . In this stage, the MLP has an input layer with three signals and two neural layers. The first one has  $N_1 = 40$  neurons, and the output neural has  $N_2 = 10$  neurons. The types of faults and the corresponding outputs of ANN are shown in columns 1 and 3 of Table 2.

The cumulants of the fault-detection stage were computed by using sliding windows with a length equal to one fundamental period, i.e., 256 samples. The dataset used for neural network training was obtained considering 128 consecutive samples from the 64th sample after the fault inception. A result of pattern generation is shown in Fig. 16, considering all the faults involving phase A. It can be noticed that the 2nd-order cumulants are calculated for all phases. In addition, it can be seen that the cumulants occupy different portions of the space according to the type of fault. Using partitions of 90 and 10 % for training and validating stages, respectively, a MSE = 0.0019 was obtained after 1,457 epochs with a hit rate of 96.8 %.

A particular result of the fault-classification stage operation is shown in Fig. 17. The fault involves phase B and ground and was simulated with  $d = 15$  km,  $R_t = 1 \Omega$ , and  $\phi = 30^\circ$ . It can be seen that the output  $y_2$ , associated with B–G faults is activated showing a B–G fault. The other outputs are identically zero. A total of 468 cases of faults were considered to test the fault-classification module. The results are shown in Table 2. As can be observed, only four cases

**Fig. 14** Fault-detection stage result for the operation of EPS with nominal frequency  $f = 60$  Hz: **a** voltage signals; **b** cumulants; **c** fault-detection result; **d** traditional methods



were erroneously classified, and the general performance of this stage shows 99.15 % of correct results.

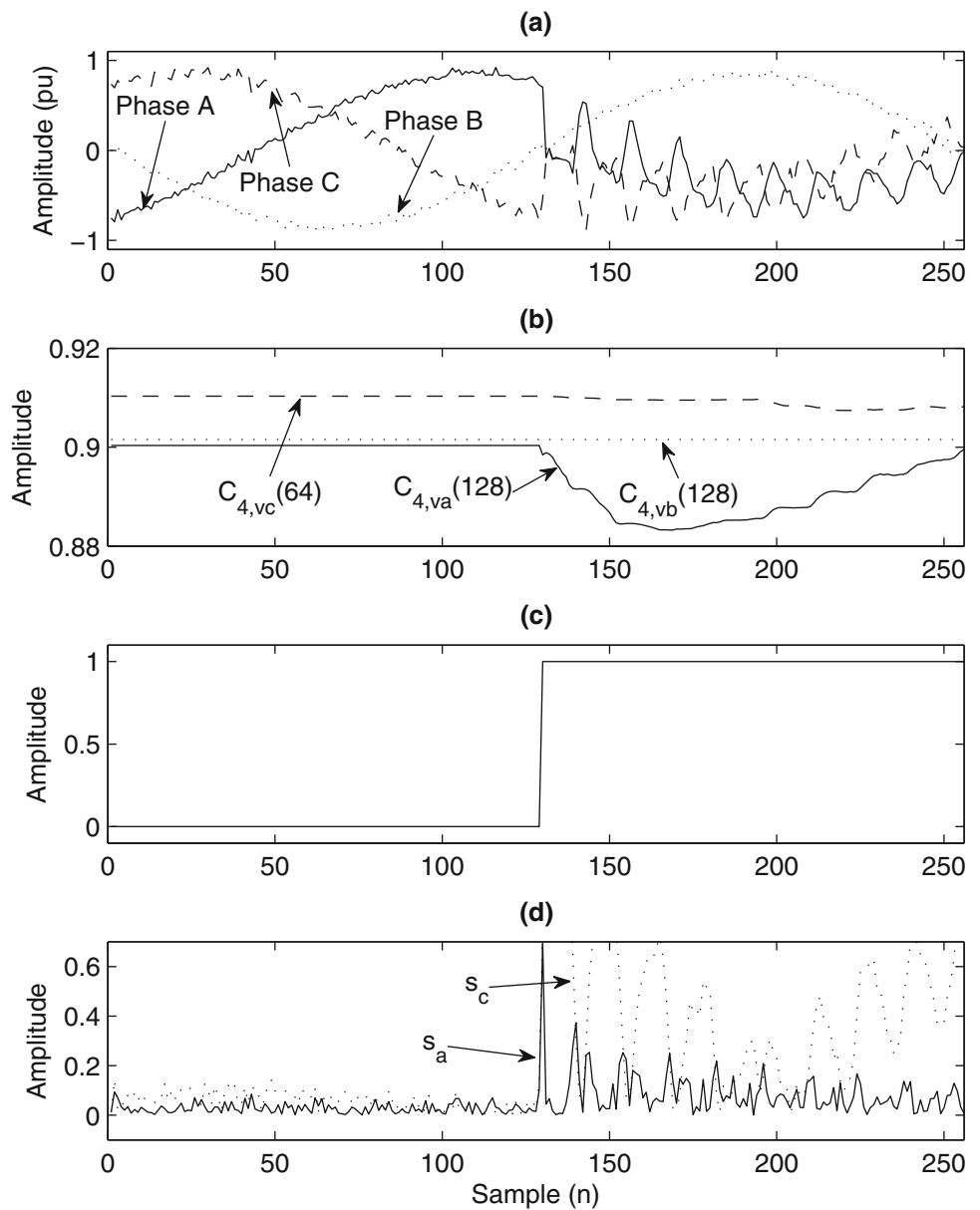
#### 4.4 Fault-Location Stage

Figure 18 shows a representation of cumulants that indicates a close relationship between the position of these statistics in the space and distance of the fault. In fact, this relationship exists and can be verified for all types of faults. Thus, ANNs can be used as a function approximation agent, instead of a pattern recognizer, to estimate the fault distance.

Considering faults involving one phase and ground (Ph-G) only, a result of the fault location is discussed in this

section. An MLP with three inputs and two neural layers ( $N_1 = 200$  and  $N_2 = 1$ ) was trained for locating faults. After the training process, a total of 100 samples were randomly chosen for validation. This result is shown in Fig. 19. It can be seen that the output of the ANN appropriately follows the curve of desired output. This result indicates that the fault distance can be correctly determined using neural networks. It must be emphasized that when operating in this stage, several samples are available for estimating the fault distance, and the result can be accurately and precisely determined from the statistical analysis of the neural network output. Finally, in this case, the last half cycle of the first fundamental period after fault inception was used for pattern generation.

**Fig. 15** Fault-detection stage results for the operation of EPS with frequency  $f = 61$  Hz, and in the presence of noise: **a** voltage signals; **b** cumulants; **c** fault detection result; **d** traditional methods



**Table 2** Results of the fault-classification stage

Type of fault	Total of simulations	Correct output	Correct answers
A–G	54	$y_1$	54
B–G	54	$y_2$	54
C–G	54	$y_3$	54
A–B–G	54	$y_4$	54
B–C–G	54	$y_5$	54
C–A–G	54	$y_6$	54
A–B	36	$y_7$	36
B–C	36	$y_8$	36
C–A	36	$y_9$	36
A–B–C	36	$y_{10}$	32
Total	468	Hits	464

#### 4.5 Joint Operation of the Protection Subsystems

A complete protection scheme of TL performs all the distance protection stages mentioned earlier. Taking this into account, this section deals with the joint operation of fault-detection, -classification, and -location stages. The algorithm can be synthesized as shown in Fig. 20. The evaluation of the algorithm shown in this figure is performed for a single-phase fault, involving phase A and ground (A–G fault).

Figure 21 shows a particular result of the proposed scheme simulating a real-time operation. The A–G fault has the following parameters:  $d = 105$  km,  $R_l = 10 \Omega$ , and  $\phi = 0^\circ$ . The voltage signals are presented in (a) where one pre-fault cycle and one post-fault cycle can be seen. The fault-detection system is responsible for monitoring continuously the volt-

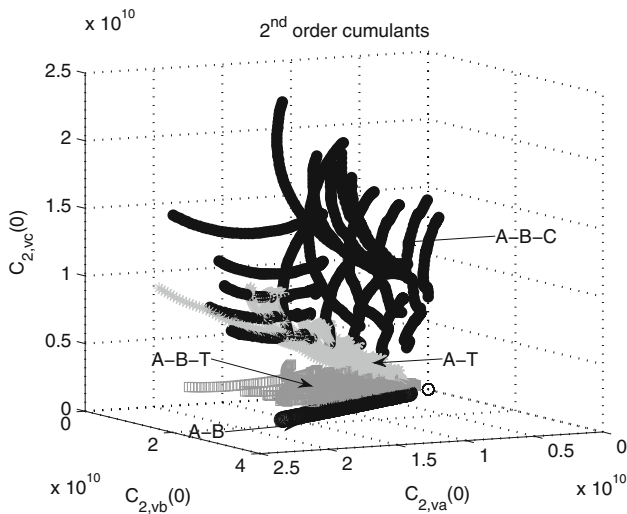


**Fig. 16** Visualizing patterns generated for fault classification

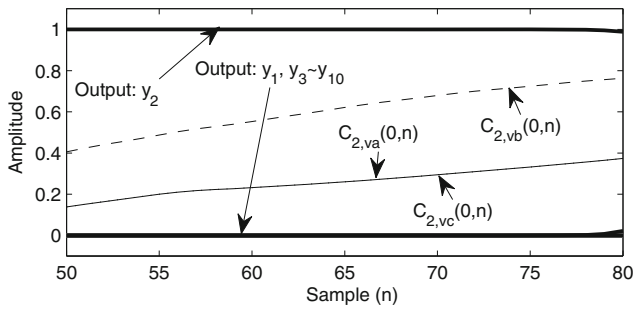


**Fig. 17** A particular result for fault classification for a B-G fault

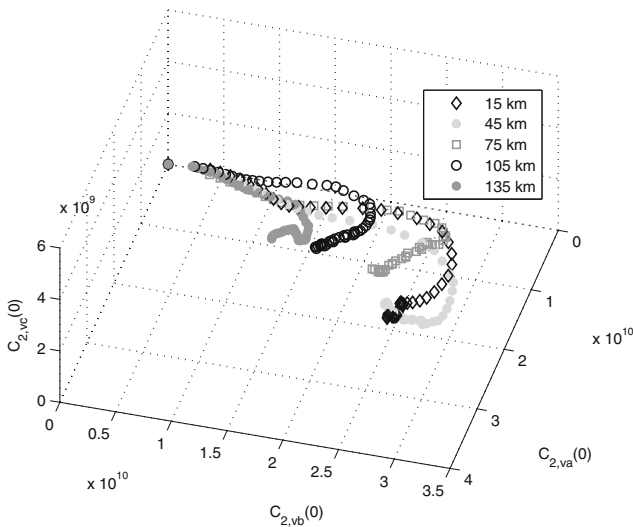


**Fig. 18** Example of the relationship between cumulants and the fault distance

age signals to identify the fault inception at sample 256. After this event, it can be observed in (b) that the fault-detection stage indicates the occurrence of the short circuit immedi-

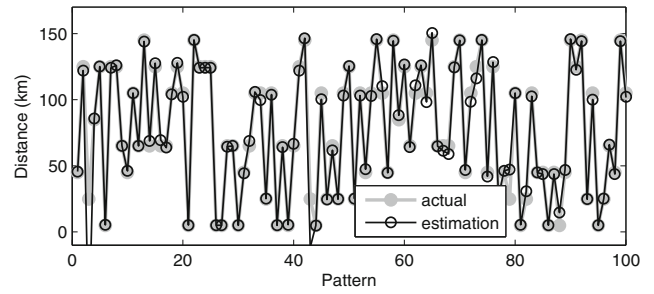


**Fig. 19** Results of validation of the ANN used for locating faults involving one phase and ground

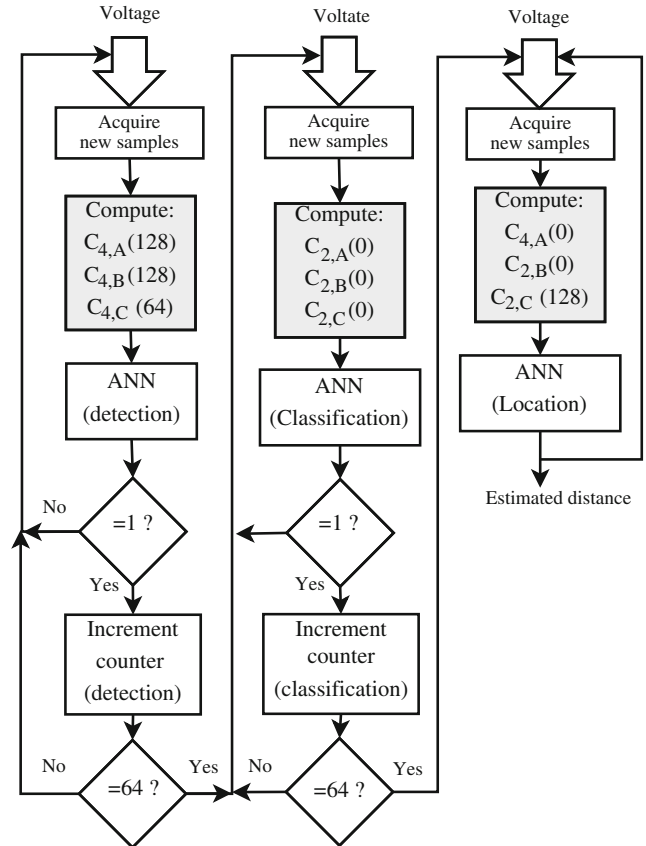
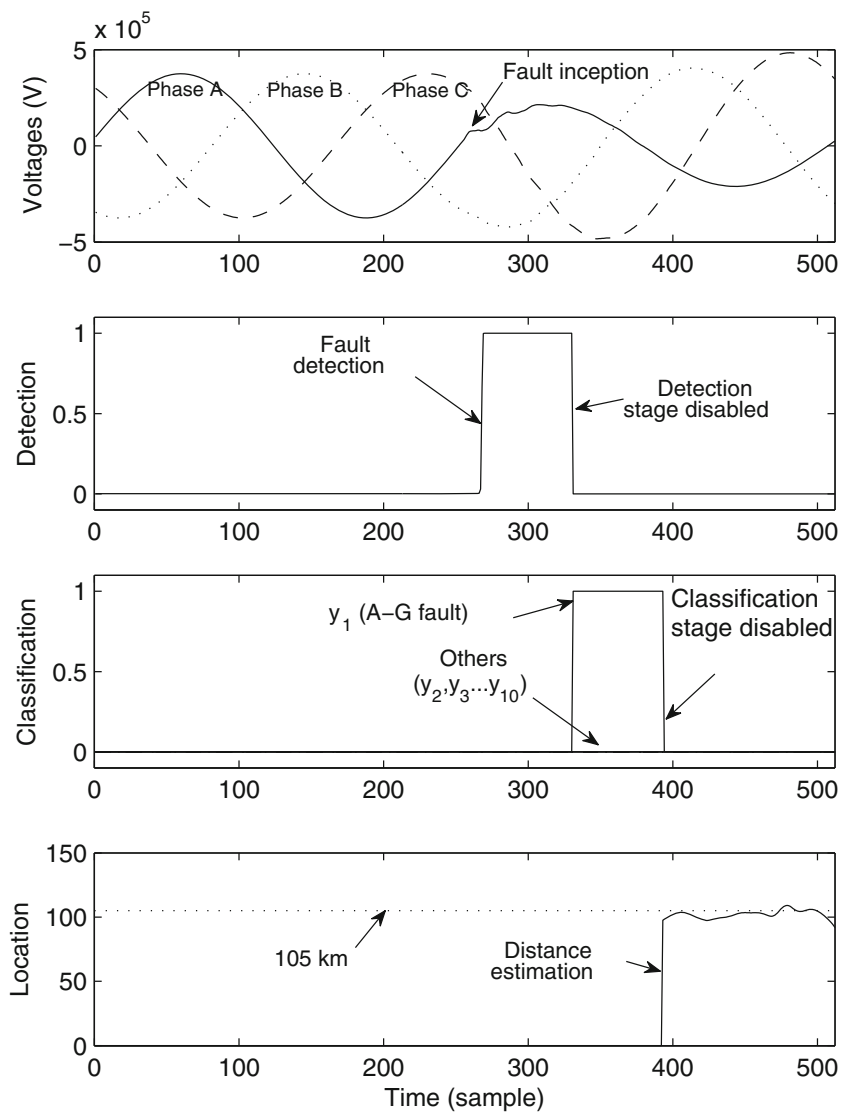


**Fig. 20** Algorithm proposed for joint operation of fault-detection, -classification, and -location stages

ately. A counter is enabled to verify the consistence of this result. After counting 64 samples consecutively, the fault-classification stage is then enabled and the fault-detection stage is disabled. In Fig. 21c, it can be verified that the output  $y_1$  is correctly activated indicating an A-G fault. The other outputs of the fault classification stage remains inactive. Again, a counter is used in the process to confirm the result. After 64 samples, the fault classification stage is disabled, and the fault-location stage is enabled. This system provides distance estimations for the simulated fault. As can be seen, the result presents good precision.

**Fig. 21** Particular result for the joint operation of fault-detection, -classification, and -location stages for an A–G fault 105 km far from the relay



The result presented in this section demonstrates one possible configuration for the protection stages of the proposed method. The counters can be adjusted considering aspects as the required speed and reliability. It must be emphasized that a relay based on the proposed algorithm could take decisions in less than one fundamental cycle (16, 67 ms). In the simulation above, considering the reach of 80 % for the primary zone of protection, the relay would send a trip signal to isolate TL2.

The traditional technique for distance protection based on the calculation of the apparent impedance was considered for comparing results. The phasors used in the impedance calculation were extracted applying the DFT of the first postfault cycle of voltage and current signals. The apparent impedance is shown in the R–X diagram of Fig. 22 (black dot). It can be observed that the impedance is out of zone 1 for a quadrilateral traditional curve. Thus, this technique requires more samples to correctly identify the fault zone. Considering the result of the proposed technique, the distance can be deter-

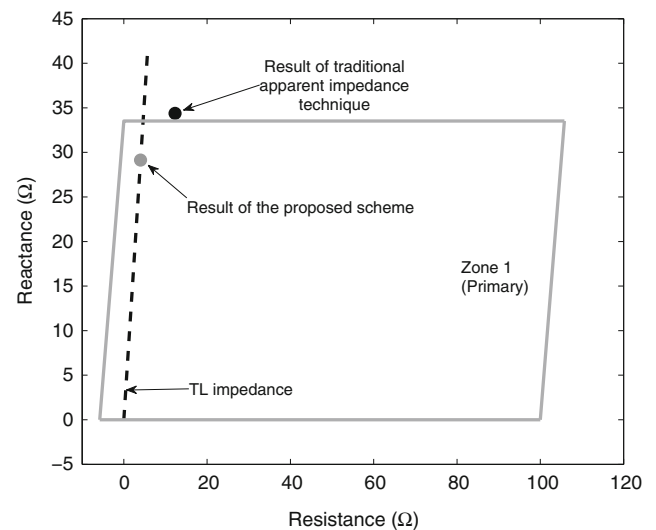


**Fig. 22** Comparison of the proposed technique with the traditional one using the calculation of apparent impedance obtained using DFT

mined by the average of the neural network estimations. Hence, the distance of the fault can be stated as 104.3 km, and in the R–X plane, it was plotted as the gray dot, as shown in Fig. 22. As can be seen, the proposed technique combines speed with consistent and precise responses.

## 5 Conclusions

This article presents a new and alternative approach for TL protection. In general, the following concluding remarks can be stated. First, the ability of quickly responding to transient components from the fault inception was responsible for fast responses. This is a basic requisite of updated protection systems. Second, the immunity to noise present in this methodology consists of an important characteristic as, in practice, real electric signals are superimposed with it. Especially in the fault-detection stage, the pre and postfault conditions must be reliably distinguished despite the noise. Finally, the use of ANN implies in an auto-adjustment system. In the fault-detection stage, for example, it is not necessary to use thresholds for correct operation. On the contrary, the network must be trained with the appropriate SNR, and the system will operate properly.

The results demonstrated that combining cumulants with ANNs could indeed be used for designing a distance relay. The individual operation of all stages of the distance protection was found to be efficient, as well its joint operation. The fault-detection process was successful in all simulated cases (100 % accuracy). In addition, 99 % of faults were correctly classified. Finally, the location procedure was successfully performed for single phase-to-ground faults.

Despite the need of using an additional algorithm for determining directionality of the fault, all the stages of the proposed scheme use voltage signals only. This characteristic implies in a methodology that is immune to common problems found in the traditional apparent impedance method. Among others, the problems caused by exponential decaying DC components and current transformer saturation are not present in this methodology. Thus, on the whole, the proposed method contributes considerably to the improvement of transmission line digital protection.

**Acknowledgments** The authors would like to thank the Electrical and Computer Engineering Department of São Carlos Engineering School (EESC-USP), the Federal University of Juiz de Fora (UFJF), and the Federal Center for Technological Education of Minas Gerais (CEFET-MG). In addition, the authors are thankful to FAPEMIG, CAPES, and CNPq for supporting this study.

## References

- Alfuhaid, A. S., & El-Sayed, M. A. (1999). A recursive least-squares digital distance relaying of transmission lines. *IEEE Transactions on Power Delivery*, *14*, 1257–1262.
- Caminha, A. C. (1977). *Introduction to electrical power systems protection*. São Paulo: Edgar Blücher. (in Portuguese).
- Chen, C. S., Liu, C. W., & Jiang, J. A. (2006). Application of combined adaptive Fourier filtering technique and fault detector to fast distance protection. *IEEE Transactions on Power Delivery*, *21*, 619–626.
- Cho, Y. S., Lee, C. K., Jang, G., & Lee, H. J. (2009). An innovative decaying DC component estimation algorithm for digital relaying. *IEEE Transactions on Power Delivery*, *24*, 73–78.
- Colonnese, S., & Scarano, G. (1999). Transient signal detection using higher order moments. *IEEE Transactions on Signal Processing*, *47*(2), 515–520.
- Coury, D. V., Oleskovicz, M., & Giovanini, R. (2007). *Digital protection of electric power systems: From the electromechanical relays to intelligent microprocessors*. São Carlos: EESC-USP. (in Portuguese).
- Coury, D. V., Oleskovicz, M., & Souza, S. A. (2011). Genetic algorithms applied to a fast distance protection of transmission lines. *Controle & Automação*, *22*(4), 495–505. (in Portuguese).
- Coury, D. V., & Jorge, D. C. (1998). Artificial neural network approach to distance protection of transmission lines. *IEEE Transaction on Power Delivery*, *11*, 102–108.
- Dalstein, T., & Kuliche, B. (1995). Neural network approach to fault classification for high speed protective relaying. *IEEE Transactions on Power Delivery*, *10*, 1002–1011.
- Dutta, A. A., & Kadu, A. N. (2010). Pattern recognition methods for detecting fault in EHV transmission lines. In *Conference on Mechanical and Electrical Technology*. Singapore.
- Eichhorn, K. F., Ladniak, L., & Lobos, T. (1993). Algorithms for digital distance protection with improved transient behavior. In *Joint International Conference: Athens Power Technology* (pp. 290–294).
- Ferreira, D. D., Cerqueira, A. S., Duque, C. A., & Ribeiro, M. V. (2009). HOS-based method for classification of Power quality disturbances. *Electronic Letters*, *45*, 183–185.
- Gerek, Ö. N., & Ece, D. G. (2006). Power quality event analysis using higher order cumulants and quadratic classifiers. *IEEE Transactions on Power Delivery*, *21*, 883–889.
- Giannakis, G. B., & Tsatsanis, M. K. (1990). Signal detection and classification using matched filtering and higher order statistics. *IEEE Transactions on Acoustics Speech, Signal Process*, *38*, 1284–1296.
- Grcar, B., Ritonja, J., Polajzer, B., & Stankovic, A. M. (2008). Estimation methods using dynamic phasors for numerical distance protection. *IET Generation, Transmission and Distribution*, *2*, 433–443.
- Haykin, S. (1999). *Neural networks: A comprehensive foundation*. Upper Saddle River, NJ: Prentice-Hall.
- Jongepier, A. G., & Sluis, L. (1997). Adaptive distance protection of double-circuits lines using ANN. *IEEE Transactions on Power Delivery*, *12*, 157–160.
- Kharpade, S. A., Kale, P. B., & Agarwal, S. H. (1991). Application of artificial neural network in protective relaying of transmission lines. In *Proceedings of the First International Forum on Applications of Neural Networks to Power Systems* (pp. 122–125).
- Marques, C. A. G. (2007). *Detection disturbance technique for Power Quality monitoring (in Portuguese)*. Master degree dissertation, Universidade Federal de Juiz de Fora.
- Mendel, J. M. (1991). Tutorial on higher-order statistics (Spectra) in signal processing and system theory: Theoretical results and some applications. *Proceedings of IEEE*, *79*, 278–305.
- Mitra, S. K. (2006). *Digital signal processing: A computer-based approach* (3rd ed.). New Delhi: Tata McGraw-Hill.
- Mohanty, S. R., Pradhan, A. K., & Routray, A. (2008). A cumulative sum-based fault detector for power system relaying application. *IEEE Transactions on Power Delivery*, *23*, 79–86.
- Osman, A. H., Abdelazim, T., & Malik, O. P. (2005). Transmission line distance relaying using on-line trained neural networks. *IEEE Transactions on Power Delivery*, *20*, 1257–1264.
- Phadke, A. G., & Thorp, J. S. (2009). *Computer relaying for power systems* (2nd ed.). Chichester: Wiley.

- Phadke, A. G., Thorp, J. S., & Adamiak, M. G. (1983). A new measurement technique for tracking voltage phasors, local system frequency and rate of change of frequency. *IEEE Transactions on Power Systems*, 102(5), 1025–1033.
- Pradhan, A. K., Routray, A., & Biswal, B. (2004). Higher order statistics-fuzzy integrated scheme for fault classification of a series-compensated transmission line. *IEEE Transactions on Power Delivery*, 19, 891–893.
- Ribeiro, M. V., Marques, C. A. G., Duque, C. A., Cerqueira, A. S., & Pereira, J. L. R. (2007). Detection of disturbances in voltage signals for Power quality analysis using HOS. *EURASIP Journal on Applied Signal Processing*, 2007, 1–13.
- Sá, J. L. P., & Pedro, L. (1991). Modal Kalman filtering based impedance relaying. *IEEE Transactions on Power Delivery*, 6, 78–84.
- Silva, I. N., Spatti, D. H., & Flauzino, R. A. (2010). *Artificial neural networks for engineering and applied sciences*. São Paulo: Artliber. (in Portuguese).
- Yu, C.-S. (2006). A discrete Fourier transform-based adaptive mimic phasor estimator for distance relaying applications. *IEEE Transactions on Power Delivery*, 21, 1836–1846.
- Zhang, N., & Kezunovic, M. (2007). Transmission line boundary protection using wavelet transform and neural network. *IEEE Transactions on Power Delivery*, 22, 859–869.